GEOLOGICA CARPATHICA, AUGUST 2023, 74, 4, 281–296 https://doi.org/10.31577/GeolCarp.2023.16

The geochemistry, origin and tectonic setting of the Tozlu metaophiolite in the Kazdağ Massif (Biga Peninsula, NW Anatolia)

FIRAT ŞENGÜN[1,2,✉], ALTUĞ HASÖZBEK[3] and GÜLLÜ DENİZ DOĞAN-KÜLAHCI[4]

[1]Department of Mining and Mineral Extraction, Çan Vocational College, Çanakkale Onsekiz Mart University, 17400, Çan-Çanakkale, Turkey; ✉firatsengun@comu.edu.tr
[2]Department of Earth Sciences, University of Gothenburg, 40530, Gothenburg, Sweden
[3]Centro Nacional de Investigación sobre la Evolución Humana (CENIEH), Burgos, Spain
[4]Hacettepe University, Geological Engineering Department, 06800 Beytepe-Ankara, Turkey

(Manuscript received May 8, 2023; accepted in revised form August 14, 2023; Associate Editor: Igor Broska)

Abstract: The Tozlu metaophiolite is composed predominantly of metagabbro, banded amphibolite, metadunite, and serpentinite, which are exposed in the Kazdağ Massif located in the northwestern part of Turkey. The geochemistry (major, trace, and rare earth elements) and petrography of the Tozlu metaophiolite in the Kazdağ Massif provided significant knowledge about protolith, petrogenesis, source characteristics and tectonic setting in northwest Turkey. Trace element geochemistry, Ti/Y (29.95–296.92 ppm) and Nb/Y (0.01–0.17 ppm) ratios suggest that metaophiolitic rocks were derived from a tholeiitic magma and igneous protolith of basaltic composition. The immobile trace element tectono-magmatic discrimination diagrams define a mid-ocean ridge basalt (MORB) to volcanic arc (IAT) affinity for the Tozlu metaophiolite. The metaophiolitic rocks demonstrate flat rare earth element (REE) patterns and enrichment of large ion lithophile elements (LILEs; i.e., Rb, Ba, Th), as well as depletion of high field strength elements (HFSEs; i.e., Nb, Th, Ti, Hf). N-MORB characteristics of the Tozlu metaophiolite on a multi-element diagram suggest that the protolith of metaophiolitic rocks generated in a subduction-related setting. The tholeiitic metaophiolitic rocks resulted from the metamorphism of an island arc-type basaltic protolith and display subduction zone components according to the Th/Yb and Ta/Yb ratios. The Tozlu metaophiolite with MORB/IAT affinity witness for supra-subduction zone originated in island arc/back-arc settings.

Keywords: metaophiolite, geochemistry, Kazdağ Massif, Biga Peninsula, NW Turkey

Introduction

Ophiolites provide important information on the reconstruction of the tectonic history of a region and indicate the presence of sutures and the closure of former oceanic basins. The ophiolitic units of Turkey and surrounding regions form a significant part of the Eastern Mediterranean region. The Eastern Mediterranean region is characterized by a great number of ophiolites and ophiolitic fragments (e.g., Şengör & Yılmaz 1981; Okay et al. 2001; Robertson 2002, 2004; Parlak et al. 2013; Çelik et al. 2019; Özkan et al. 2022; Fig. 1), which are the remnants of oceanic lithosphere involved during the Late Paleozoic–Mesozoic geodynamic evolution of the Tethys realm. These structurally-intact, ophiolitic fragments show distinct spreading ages, including the timing of genesis and emplacement. And so, based on their protolith ages, which were recorded from west to east, it can be concluded that these units are (1) the relics of the Jurassic oceanic lithosphere (Dinaride–Hellenide–Albanide ophiolites), which exhibit the former existence of one or two major oceanic basins (e.g., Robertson 2002, 2012; Liati et al. 2004; Gartzos et al. 2009; Höhn et al. 2022); (2) Lower Jurassic to Upper Cretaceous ophiolites, which are widespread in Turkey (Taurides, Pontides, Anatolides), Cyprus, and Syria (Parlak & Delaloye 1999; Robertson 2002; Çelik et al. 2006; Parlak et al. 2013; Topuz et al. 2013; Robertson et al. 2014); and (3) Lower to Middle Jurassic ophiolites from the Lesser Caucasus (Galoyan et al. 2009; Rolland et al. 2009; Sosson et al. 2010; Hassig et al. 2013). These ophiolitic units reflect the evolutionary stages of Neotethyan ocean basins from the Jurassic to Cretaceous (e.g., Robertson 2002; Dilek et al. 2007; Robertson et al. 2009; Topuz et al. 2013; Çelik et al. 2019; Özkan et al. 2022). Although the northwestern Turkey region exposes ophiolites with well-preserved magmatic and metamorphic records (especially on the Biga Peninsula), their protolith ages and tectonic settings have not yet been determined. Northwestern Turkey plays an important role in the understanding of the geodynamic history of larger regions, since it provides a geographic link between the main ophiolitic units in the Eastern Mediterranean region. However, a general framework remains missing due to a lack of isotopic age data and geochemical data.

In this study, we focus on well-preserved metagabbros from the Tozlu metaophiolite in the Kazdağ Massif, which are located in northwestern Turkey. New, whole-rock, geochemical, major, and trace element analyses from the metagabbros

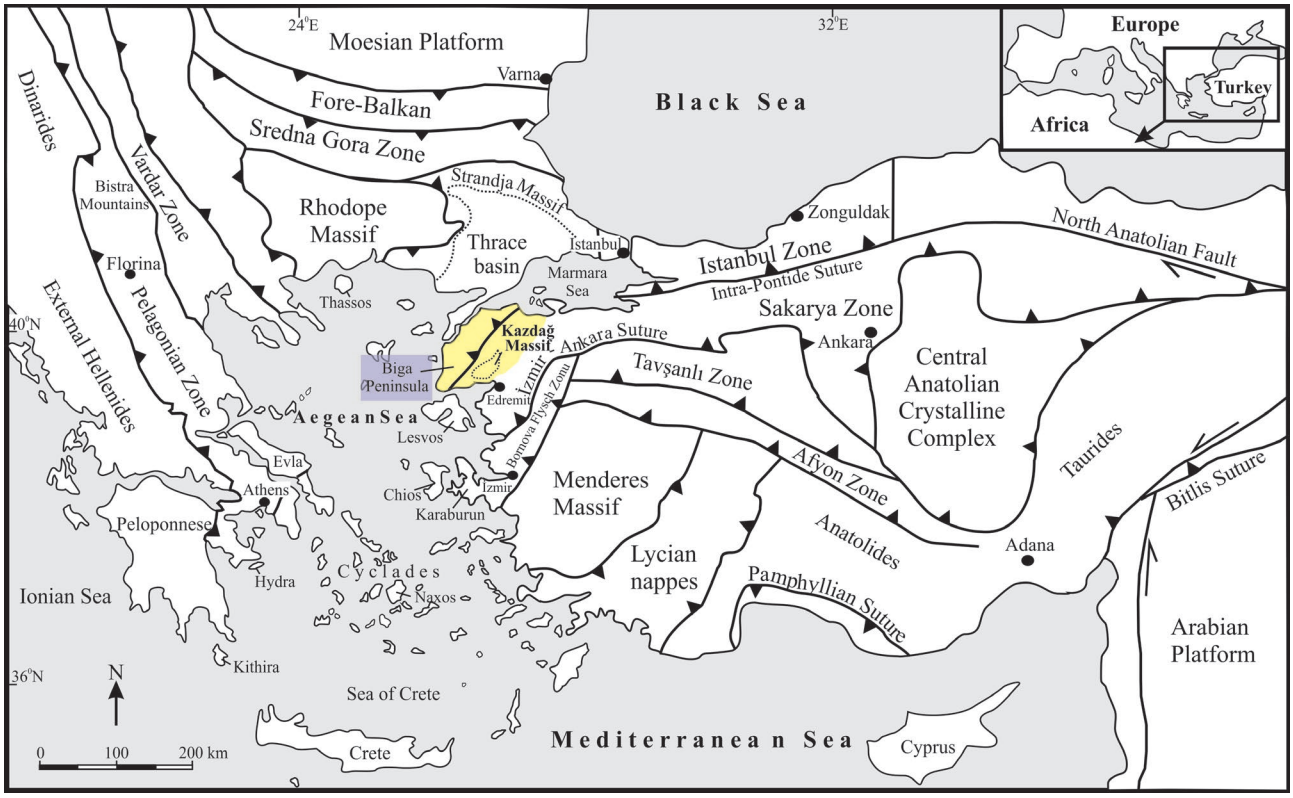

Fig. 1. Tectonic map of the Eastern Mediterranean region showing the major geotectonic units and the bounding sutures (modified from Okay et al. 2006; Meinhold et al. 2010).

have been used to evaluate the primary tectonic setting of formation of the oceanic lithosphere materials. The purpose of this paper is to give insight into geochemical signature of metagabbros in the high-grade metamorphic basement of the Kazdağ Massif and reveal the origin, source characteristics and tectonic settings, which could contribute to the Tethyan geodynamic evolution of Turkey.

Geological background

Regional geology

Northwestern Anatolia is characterized by the ophiolite emplacement, arc magmatism, high pressure/low temperature metamorphism, subduction, and continent–continent collision processes that took place during the Late Cretaceous–Early Eocene period (Okay & Tüysüz 1999). The Istanbul Zone and Strandja Zone collided as a result of the closure of the Intra-Pontide Ocean in the Late Cretaceous. The Sakarya Zone in northwestern Anatolia is a tectonic mosaic that includes several tectonic units of continental and oceanic assemblages of different origin and ages, which is separated by suture zones that represent the closure of branches of Tethyan ocean basins (e.g., Şengör & Yılmaz 1981; Okay & Tüysüz 1999). The Strandja Massif and the Thrace Basin border the Biga Peninsula, one of these larger units that occur at the western end of the Sakarya Zone to the north, and the Aegean Sea marks the western and southern borders (Fig. 2). To the south, the Izmir–Ankara–Erzincan suture (IAES) zone separates the composite continental blocks of the Pontides (Sakarya Zone, Rhodope–Strandja Zone, Istanbul Zone, eastern Pontides) from the composite Anatolide–Tauride Block. The IAES represents the remnants of an oceanic domain that was consumed by northward subduction under the Pontides from the late Paleozoic to the late Mesozoic with continental collision during the Paleocene–early Eocene period (e.g., Robertson 2002; Ustaömer & Robertson 2010; Topuz et al. 2013; Okay et al. 2018; Özkan et al. 2022).

Geological outline of the Biga Peninsula

The Biga Peninsula in NW Turkey lies in the Alpine orogenic system of the eastern Mediterranean region and mainly consists of plutonic and associated volcanic rocks, ophiolites, and high-grade metamorphic rocks. The Intra-Pontide suture (Fig. 2) separates these different tectonic assemblages from each other. These units belong to the Rhodope–Strandja Massif to the north and to the Sakarya Zone to the south. The Peninsula includes the following main units: (i) a Variscan basement of high-grade metamorphic rocks of the Kazdağ Massif (Okay & Satır 2000a, b; Duru et al. 2004, 2012; Erdoğan et al. 2013), greenschist-facies rocks of the Çamlıca metamorphic unit (Şengün et al. 2011), and the Kemer metamorphic unit

(Late Cretaceous; Beccaletto et al. 2007; Aygül et al. 2012). The metamorphism was Carboniferous (330–308 Ma) in age (Okay et al. 1996; Okay & Satır 2000b) and these metamorphic rocks were intruded by Devonian/Carboniferous (401–336 Ma) granites (Okay et al. 1996; Aysal et al. 2012; Sunal 2012; Şengün & Koralay 2017; Şengün et al. 2020); (ii) the Triassic–Lower Jurassic units of the Karakaya Complex exposed only in the eastern part of the Biga Peninsula (Okay & Göncüoğlu 2004); (iii) the subduction–accretion Çetmi mélange (Early Cretaceous; Okay et al. 1991; Beccaletto et al. 2005); (iv) the Permo–Triassic Ezine Group, which is tectonically overlain by Lower Cretaceous Denizgören ophiolite (Beccaletto & Jenny 2004); (v) Tertiary sedimentary cover units that unconformably overlie all of the units mentioned above (Fig. 2).

The Kazdağ Massif lies in the Sakarya Zone and is located on the southernmost part of the Biga Peninsula in northwest Turkey. The Kazdağ Massif forms structurally NE-plunging and NE–SW-trending anticlinorium. High-grade metamorphic rocks, which occur on the core of the anticlinorium, typically resemble a gneissic dome. The Kazdağ Massif is generally regarded as the latest Oligocene metamorphic core complex (e.g., Okay et al. 1991; Okay & Satır 2000b; Duru et al. 2004) and can be correlated to the Rhodope Massif in Greece in terms of lithology and the timing of metamorphism (Okay et al. 1996, Okay & Satır 2000b; Beccaletto & Jenny 2004). The Kazdağ Massif is subdivided into four formations (Duru et al. 2004; Fig. 3). These are, from the base to the top: (i) the Fındıklı formation, which consists of an intercalation of amphibole-bearing gneiss, quartz–feldspathic gneiss, marble, and amphibolite; (ii) the Tozlu metaophiolite, which is mainly composed of metaophiolitic rocks including metagabbro, metapyroxenite, metadunite, and serpentinite; (iii) the Sarıkız unit, which consists of platform-type, highly-recrystallized white marbles with gneiss horizon; (iv) the Sütüven Formation, which forms the uppermost part of the Kazdağ Massif and comprises quartz–feldspathic gneisses with a lesser amount of amphibolite, marble horizons, and lenses. The dominant lithology of quartz–feldspathic gneisses is made up of sillimanite gneiss, muscovite gneiss, and granitic gneiss based on the field observations. Moreover, migmatization is widely observed in the quartz–feldspathic gneisses of the Sütüven Formation. The Sütüven Formation is intruded by the Oligo–Miocene granodiorite.

The metamorphic rocks of the Kazdağ Massif underwent amphibolite to granulite-facies metamorphism under progressive compression during the Alpine orogeny, which had been associated with the emplacement of metagranites (Okay & Satır 2000b; Erdoğan et al. 2013). Zircon ages from the felsic gneisses and amphibolite in the Kazdağ Massif, which is determined by the single-zircon stepwise Pb-evaporation method, is 308±16 Ma and 329±5 Ma, respectively. These ages suggest that the high-grade metamorphism in the Kazdağ Massif is Carboniferous in age (Okay et al. 1996). However, K–Ar mica ages from two gneisses in the Kazdağ Massif yielded 26±3 Ma and 27±3 Ma that were related to the Alpine overprint (Bingöl 1969). Okay & Satır (2000b) reported Rb/Sr muscovite and biotite ages clustering at 24–20 Ma and

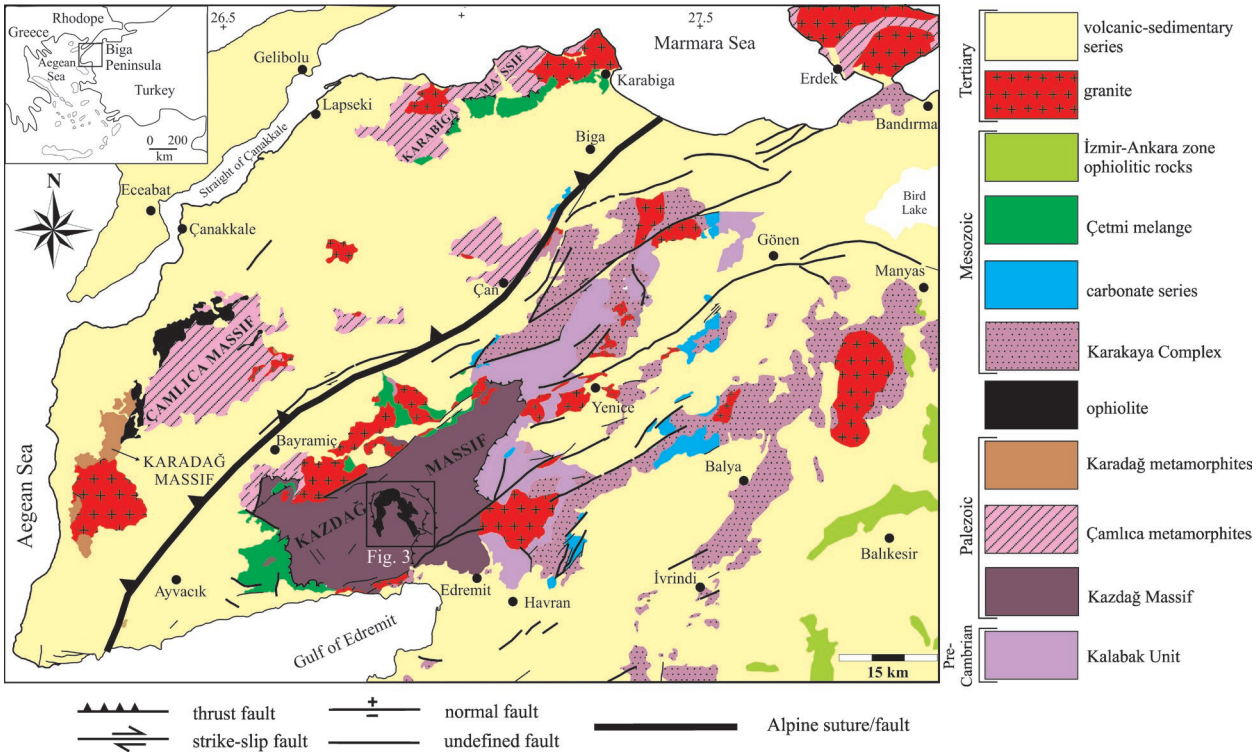

Fig. 2. Generalized geological map of the Biga Peninsula (modified from MTA 2012). Inset map shows location of the Biga Peninsula.

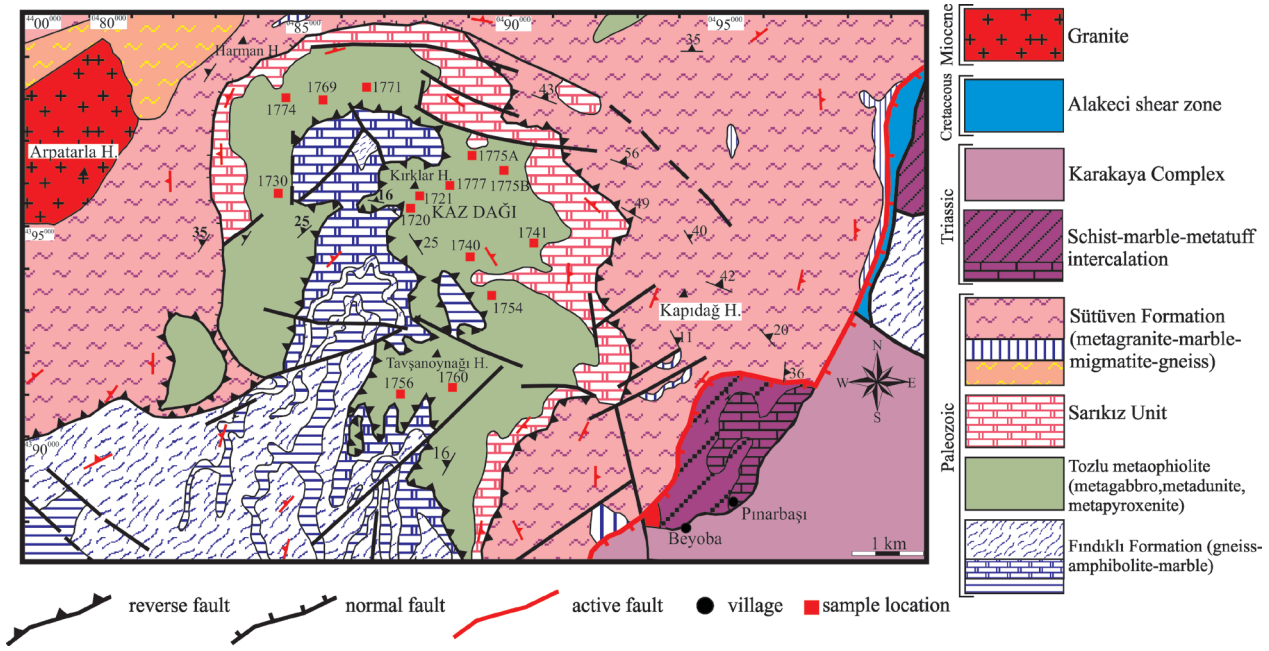

Fig. 3. Detailed geological map of the high-grade metamorphic rocks in the Kazdağ Massif (modified from Duru et al. 2012).

20–18 Ma from the gneiss samples, respectively. More recently, U–Pb zircon ages from metagranite samples yielded 24.8±4.6 Ma and 28±10 Ma, which were interpreted as the timing of the migmatitic magmatism in the Kazdağ Massif that occurred during the Alpine orogeny (Erdoğan et al. 2013). These isotopic data suggest that high-grade metamorphism in the Kazdağ Massif occurred during the Carboniferous and during the late Oligocene (Okay et al. 1996; Okay & Satır 2000b; Erdoğan et al. 2013). Apatite fission-track ages of 17–14 Ma from the Alakeçi shear zone located on the western flank of the Kazdağ Massif were linked to exhumation of the Kazdağ Massif (Cavazza et al. 2009). The P–T conditions of the high-grade metamorphism have been estimated at 5±1 kbar and 640±50 °C (Okay & Satır, 2000b). However, the P–T conditions of Tozlu metaophiolite were determined as 646 °C at 9 kbar, which reflects the metamorphic temperature related to the amphibolite-facies metamorphism (Şengün & Zack 2016).

Field characteristics

The Tozlu metaophiolite is mainly composed of metagabbro, metadunite, metapyroxenite, and serpentinite (Fig. 3). Metagabbro forms the dominant rock type within the Tozlu metaophiolite and occurs as layers of varying thickness, which alternates with amphibolite and metadunite. The metagabbro is black-colored, coarse-grained (0.5 to 0.8 mm), well-foliated, and banded (Fig. 4a). These layers of metagabbro are illustrated by alternating plagioclase and amphibole-rich bands (Fig. 4b). Tectonic lenses consisting of marble–amphibolite–quartz–feldspathic gneiss intercalations occur within the metagabbro and metadunite. These tectonic lenses were deformed together with the units (Fındıklı, Sarıkız, Sütüven formations) as taking the present position of the Tozlu metaophiolite and during the later deformations. Outcrop distribution of rock units forming the Tozlu metaophiolite and structural observations indicate that the Tozlu metaophiolite is composed of recumbent folds, which are overturned to southern and tectonic slices.

Amphibolites appear black-colored, medium to coarse-grained (0.3 to 0.6 mm), showing a well-developed foliation and they may refer initially lava flows (Fig. 4c). Amphibole and plagioclase can be observed in hand specimens. Metadunite alternating with metagabbros and amphibolite has a yellowish-green color, as well as a massive structure and readily-identifiable olivine crystals (Fig. 4d).

The Tozlu metaophiolite tectonically lie above the marble of the Fındıklı Formation occurring on the central part of the Kazdağ dome (Fig. 3). Marbles are broadly overlain by metagabbros, whereas the metadunite overlies the marble on the western side of the marble core. This tectonic relation is a thrust developed prior to metamorphism. The Tozlu metaophiolite is unconformably overlain by the Sarıkız unit, which is represented by thick platform-type, highly-recrystallized, white marbles that alternate with migmatized metasedimentary rocks. This contact is characterized by basal conglomerates. The relationship between these two units was also regarded as an angular unconformity before thrusting (Duru et al. 2004; Erdoğan et al. 2013). The basal conglomerates are observed between the Tozlu metaophiolite and the Sarıkız unit around the Sarıkız hill, as well as the southern and western side of the Kazdağ dome. The Sarıkız unit starts with basal conglomerate (thickness of up to 5 meters) at the lowest part

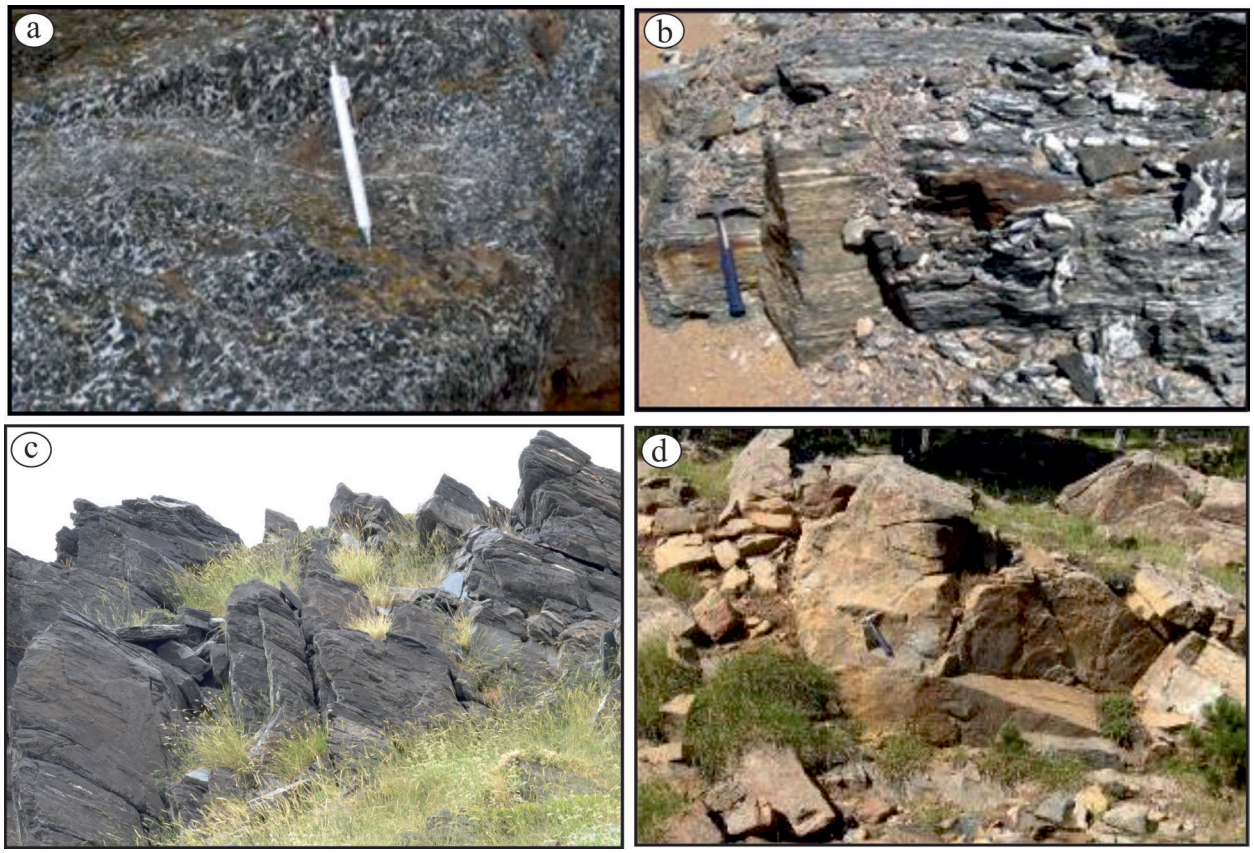

Fig. 4. Field photographs from the Tozlu metaophiolite: **a** — general view of black-colored, coarse-grained metagabbro; **b** — banded metagabbro; **c** — well-foliated, banded amphibolite; **d** — green-colored, massive metadunite.

with fragments from the Tozlu metaophiolite. It passes upward with gray-colored, fine- to medium-layered metasedimentary rocks. These metasedimentary rocks pass gradationally upward into white-colored marbles, which shows the presence of clastic succession on the lower part of the Sarıkız unit. Coarse grains in gneiss between metasedimentary horizons are mainly composed of quartz and feldspar.

Analytical methods

Fresh samples were collected from the Tozlu metaophiolite, taking care to avoid weathered, hydrothermally-altered, or mineralized pieces. Fourteen representative samples were selected from the metagabbros (10 samples) and metadunite (4 samples), and analyzed for major, trace and rare earth elements (REE) chemical composition. The location of the rock samples is shown in Fig. 3.

Whole-rock chemical analyses were conducted by analytical facilities at the ALS Chemex Laboratory in Canada and calibrated against internal and international standards. Trace element and REE concentrations were determined by Inductively Coupled Plasma – Mass Spectroscopy (ICP-MS). Major oxides were analyzed by Inductively Coupled Plasma – Atomic Emission Spectroscopy (ICP-AES). The prepared sample (0.200 g) was added to lithium metaborate/lithium tetra borate flux (0.90 g), mixed well, and then fused in a furnace at 1000 °C. The resulting melt was then cooled and dissolved in 100 mL of 4 % nitric acid 2 % hydrochloric acid. This solution was then analyzed by ICP-AES and the results were corrected for spectral inter-element interference. The oxide concentration was calculated from the determined elemental concentrations.

Petrography

Metaophiolitic rocks exposed on the Kazdağ Massif are characterized by metagabbro, metadunite, metapyroxenite and serpentinite. The mineral assemblage of metagabbros is dominated by plagioclase (~40 vol. %), hornblende (~30 vol. %), clinopyroxene (~15 vol. %), and orthopyroxene (~10 vol. %) (Fig. 5a, b). Accessory mineral phases include epidote, chlorite, quartz, rutile, sphene, zircon, and ilmenite. Inclusion of quartz, epidote, and zircon occur in clinopyroxene minerals. The most conspicuous textures of the metagabbros are granonematoblastic and poikiloblastic. Plagioclase is very common, medium to coarse, lath-shaped, and exhibit polysynthetic twinning. Hornblende is coarse-grained, with pleochroism of colorless to light green and green to greenish-brown.

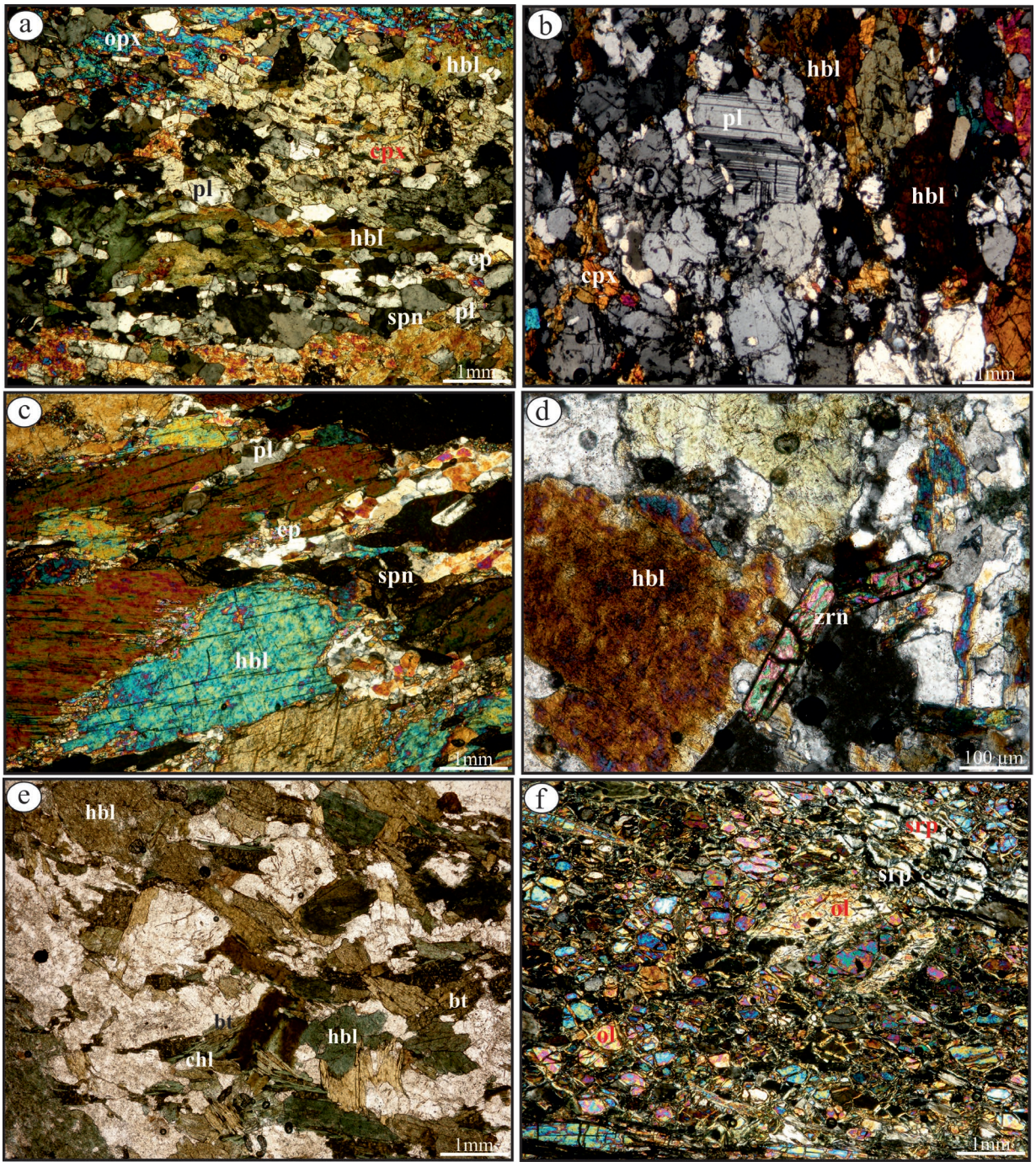

Fig. 5. Photomicrographs of selected metaophiolitic rocks: **a** — texture of metagabbro; **b** — amphibolite represented by elongated hornblende and plagioclase grains; **c** — biotite replaced by chlorite showing greenschist-facies overprint in amphibolite; **d** — texture of metadunite (hbl – hornblende, cpx – clinopyroxene, opx – orthopyroxene, pl – plagioclase, bt – biotite, spn – sphene, ep – epidote, chl – chlorite, ol – olivine, srp – serpentine; mineral abbreviations after Whitney & Evans 2010).

Clinopyroxene is more abundant (~15 vol. %) and occurs as medium to coarse subhedral grains, which are frequently replaced by epidote and hornblende. Orthopyroxene is of limited abundance (~10 vol. %) and pleochroic from pale pink to pale green.

Hornblende (~50 vol. %), plagioclase (~35 vol. %), quartz (~5 vol. %), biotite (~5 vol. %) represent the main mineral assemblage of the amphibolites (Fig. 5c, d). Accessory and secondary mineral phases are mainly composed of epidote, chlorite, biotite, Ca-amphibole, sphene, zircon, apatite, and ilmenite. Hornblende forms the dominant mafic mineral phase in amphibolites and shows subhedral crystal forms (Fig. 5c). Prismatic to elongated hornblende crystals show intergrowth with latter mineral phases. Plagioclase crystals are typically

very common, fine-grained, subhedral grains. Pseudomorphic replacement of biotite by chlorite (Fig. 5e), and rutile enveloped by titanite indicate the gradual retrogression to greenschist-facies. The dark green, elongated hornblende minerals microscopically refer to the lepidoblastic texture and macroscopically define foliation in the amphibolites. Green-colored, massive metadunites have the main mineral composition of olivine, serpentine, and magnetite, with a lesser amount of pyroxene, calcite, tremolite, and talc (Fig. 5f). Metadunite samples were mostly serpentinized. According to the textures and mineral assemblages, the Tozlu metaophiolitic rocks underwent the amphibolite-facies to greenschist-facies metamorphism; the latter indicated by the chloritization of biotite and amphibole crystals, including sphene rims around the rutile crystals.

Whole-rock geochemistry

The whole-rock major oxide and trace element compositions of fourteen selected metaophiolite samples (metagabbro and metadunite) from the Tozlu metaophiolite in the Biga Peninsula are listed in Table 1. If the loss of ignition (LOI) values are usually less than 2 wt. %, the low alteration took place on samples (e.g., Polat et al. 2002). The LOI values of metagabbros (10 samples) range from 0.6 to 1.80 wt. %. However, metadunites (4 samples) have LOI values of 4.6–9.8 wt. %, which suggests the presence of secondary hydrated and carbonate phases (Table 1).

The Tozlu metaophiolite experienced regional amphibolite-facies metamorphism. Some major elements (Si, Na, K and Ca) and trace elements (Rb, Sr, Cs, Ba and U) in basaltic rocks are known to be mobile during magmatism and metamorphism (e.g., Sun & Nesbitt 1978). However, immobile trace elements (Y, Zr, Nb, Ta, Hf) and REE could be used for reliable petrogenetic interpretations and tectono-magmatic discriminations of metaophiolitic rocks. Therefore, variation diagrams using higly-immobile Zr as a discrimination index were depicted to reveal the element mobility and geochemical trends. The variations binary diagrams exhibit clear linear trends and a good correlation with Zr for major and trace elements, which have immobile behaviour during metamorphism and alteration (Fig. 6). MgO an TiO_2 indicate linear correlation and increase as Zr decreases (Fig. 6a, b). However, Al_2O_3 and CaO show scattered trends on these variation diagrams, which suggests their mobility (Fig. 6c, d). Trace elements (e.g., Nb, Y, Hf, Zr) and REE, which do not behave in a mobile trend during metamorphism and alteration, are plotted against Zr and indicate strong linear trends (Fig. 6e–h). This immobile behaviour of the major oxides and trace elements, except for Al_2O_3 and CaO, reflects the magmatic origin and demonstrate igneous differentiation trends.

The metagabbros have basic chemical compositions with SiO_2 (43–54 wt. %; Table 1). They are characterized by MgO contents of 7.53–13.2 wt. % and TiO_2 concentrations ranging from 0.22 to 1.44 wt. %. CaO content is high (10.7–15.9 wt. %). They have low K_2O (0.04–1.4 wt. %), high Na_2O (1.4–2.53 wt. %), and high Al_2O_3 (8.4–17.8 wt. %) contents. Their Mg# values vary from 77 to 89 and are markedly higher than the reference value for primary basaltic magma (Frey et al. 1978). The metagabbro samples are enriched in CaO, thereby exhibiting that Ca-amphibole and epidote are abundant in their mineralogical composition. High Al_2O_3 concentrations may result from plagioclase abundance in metagabbros. However, the metadunites have ultrabasic compositions of SiO_2 (37–42 wt. %). These samples are characterized by high MgO (34.8–40.9 wt. %), low CaO (0.71–2 wt. %), Al_2O_3 (0.84–2.21 wt. %), and TiO_2 (0.01–0.05 wt. %) contents.

With the exception of three samples (samples 1740, 1760, 1777), the metagabbros have high Zr (62–128.7 ppm), Hf (1.7–3.6 ppm), Th (0.3–5.1 ppm), and Nb (1.2–4.2 ppm) concentrations. These three samples (sample 1740, 1760, 1777) show depletion in some HFSEs (high field strength elements), such as Zr contents (7–16 ppm), Hf contents (0.3–0.5 ppm), Th contents (0.05 ppm), and Nb contents (0.2–0.4 ppm). The abundance of compatible elements in metagabbros is characterized by a Ni content of 113–240 ppm, Co content of 31.7–76.5 ppm, and Cr content of 310–580 ppm. The metadunite samples indicate major and trace element characteristics typical for a peridotite, such as low SiO_2, and very high MgO, Cr, and Ni concentrations (Table 1).

The protolith of metaophiolite is classified as basalt, except for one sample (sample 1721 from metadunites) according to the Zr/Ti versus Nb/Y classification diagram of Pearce (1996) (Fig. 7a). The metagabbro samples fall between island arc tholeiite and calc-alkaline areas according to the diagram of Th versus Co (Fig. 7b). The geochemical affinity of the metaophiolite samples was illustrated in the discriminant diagram of P_2O_5 versus Zr, which shows that most of the metaophiolite samples have a tholeiitic character (Fig. 7c). The low Zr/Y (0.21–7.99) and Zr/Ti (0.001–0.05) ratios confirm the tholeiitic affinity.

On the N-MORB normalized multi-element incompatible trace element diagram, metagabbros exhibit slight enrichment of large ion lithophile elements (e.g., Rb, Ba, Th, Sr) relative to HFSEs (e.g., Nb, Zr, Hf; Fig. 8a). However, metadunite samples indicate strong Sr depletion and slight Hf enrichment. The metagabbro samples exhibit positive Sr anomalies that may reflect plagioclase accumulation in some samples and/or may represent the arc-type signature of partial melting. Most of the metaophiolite samples show conspicuous negative Nb and Zr anomalies at higher abundances relative to N-MORB. Negative Zr and Nb anomalies are elucidated by protecting immobile elements (Pearce & Peate 1995), which reflects the depletion of mantle wedge source during partial melting (Wilson 1989). N-MORB characteristics and Nb–Ti–Zr depletions of metaophiolitic rocks (Fig. 8a) demonstrate that the protolith of metaophiolitic rocks formed in a subduction-related setting or it may be originated from a mantle source modified by the earlier subduction. The low Ce/Pb (0.10–0.47; 0.22–2.82) and high Ba/Nb (7.5–37; 2.06–208) ratios in metadunite and metagabbro samples reflect the influx of slab

Table 1: Major (wt. %) and trace element (ppm) analyses of metaophiolitic rocks from the Tozlu metaophiolite.

	Metadunite				Metagabbro									
Sample no.	**1720**	**1721**	**1730**	**1774**	**1740**	**1741**	**1754**	**1756**	**1760**	**1769**	**1771**	**1775A**	**1775B**	**1777**
Major elements (wt. %)														
SiO_2	37.4	38.7	42.6	41.9	47.5	44.2	46.7	48.3	48.9	54.2	43.7	44.8	44.2	51.7
Al_2O_3	0.84	2.21	2.07	1.88	15.8	17.1	16.8	14.9	16.6	8.4	17.8	17.8	16.9	16.3
Fe_2O_3	12	8.09	8.56	8.12	6.22	11.1	8.47	9.73	5.8	7.5	8.3	7.8	9.2	5.6
CaO	1.35	1.68	0.71	2	12.5	13.8	13.4	11	13.9	10.6	15.9	15.2	14.5	12.6
MgO	40.9	36.9	35.8	34.86	11	8.72	11.05	7.53	10.2	13.2	9.2	10.3	10.7	8.6
Na_2O	0.05	0.08	0.02	0.07	2.11	1.83	1.69	2.53	2.16	1.4	1.5	1.5	1.9	1.9
K_2O	0.01	0.01	0.03	0.01	0.05	0.35	0.19	0.1	0.04	1.4	0.1	0.2	0.2	0.1
Cr_2O_3	0.17	0.36	0.35	0.333	0.07	0.05	0.08	0.04	0.04	0.1	0.0	0.1	0.0	0.0
TiO_2	0.01	0.04	0.05	0.04	0.22	1.37	0.78	1.44	0.31	0.6	1.1	0.7	0.8	0.4
MnO	0.2	0.12	0.11	0.11	0.12	0.17	0.17	0.15	0.12	0.2	0.2	0.1	0.2	0.1
P_2O_5	0.01	0.01	0.06	0.01	0.02	0.1	0.03	0.2	0.02	0.1	0.0	0.0	0.0	0.01
LOI	4.66	8.46	12.8	9.8	1.49	1.1	1.79	1.59	0.6	1.8	1.6	1.1	1.0	1.6
Total	*97.6*	*96.7*	*103.2*	*99.1*	*97.1*	*99.9*	*101.2*	*97.5*	*98.7*	*99.5*	*99.5*	*99.6*	*99.7*	*98.8*
Mg#	94	95	95	95	89	78	85	77	89	89	83	85	84	87
Trace elements (ppm)														
Ba	4.7	3.1	7.4	3	7.1	14.8	11.8	14.1	3.1	710	7	7	11	4.6
Co	135.5	113.5	111.5	105.6	43	45.5	43.3	43.2	36.9	76.5	68.1	58.4	67.4	31.7
Cr	1330	2720	2740	2685	480	330	580	310	320	380	375	420	445	370
Cs	0.15	0.07	0.02	0.1	0.01	2.01	0.64	0.04	0.13	0.2	0.1	0.2	0.1	0.05
Cu	57	5	5	2.3	73	5	5	28	63	116.6	200.8	6.7	24.9	25
Ga	1.7	2.6	2.6	1.4	11.9	17	17.4	17.8	11.8	10.1	17.8	16.7	17.5	15.2
Hf	0.2	0.2	0.2	0.1	0.3	2.6	1.7	2.7	0.3	3.6	2.1	2.2	2.4	0.5
Nb	0.2	0.2	0.2	0.4	0.2	4.2	2.4	4.2	0.2	3.4	3.4	1.2	0.8	0.4
Ni	2370	2240	2670	1954	232	119	240	150	184	174	113	152	129	120
Pb	7	5	5	1.5	5	5	18	5	5	6.2	13.1	10.6	4.7	5
Rb	0.2	0.5	0.2	0.3	0.6	12.2	4.5	2.5	0.6	27.3	1.3	2.5	1.9	1.3
Sr	33.5	14.4	2.7	12.9	78.1	526	341	170.5	105	331.8	258.3	313.6	169.4	120.5
Ta	0.1	0.1	0.1	0.1	0.1	0.3	0.1	0.3	0.1	0.3	0.3	0.1	0.1	0.1
Th	0.05	0.07	0.05	0.2	0.05	0.32	0.12	0.32	0.05	5.1	0.3	0.5	0.5	0.05
U	0.05	0.05	0.05	0.1	0.05	0.12	0.66	0.12	0.05	1.6	0.2	0.2	0.1	0.05
V	23	5	49	52	115	311	253	314	165	182	271	248	266	189
Y	2	2.9	1.2	2.4	16	30	19.5	31.7	29.3	16.1	22.2	18.3	21.8	12.9
Zn	70	56	48	36	40	83	73	58	37	40	35	8	8	47
Zr	1	3	2	0.5	27	76	62	88	38	128.7	82.7	87.7	96.5	16

Mg# = 100 Mg/(Mg + Fe^{2+}), assuming Fe^{2+} = 0.84 total Fe

fluids/melts into the mantle wedge respectively. Nb, Ti, Zr, P depletions, low Ce/Pb (0.10–2.82) and high Ba/Nb (2.06–208) ratios in metaophiolite are the characteristics for the subduction zone magmatism. Metadunite samples indicate N-MORB normalized trace element profile similar to metagabbro samples, as well as an analogous LREE-depleted (Nd and Ce) chondrite-normalized pattern.

Rare earth element concentration of metaophiolite samples are given in Table 2. The chondrite-normalized REE patterns of most metaophiolite samples are generally uniform, except for one metagabbro sample (sample 1769), and are characterized by relatively flat middle rare earth elements (MREE) to heavy rare earth elements (HREE), including slightly enriched or depleted light rare earth elements (LREE; Fig. 8b). One metagabbro sample (1769) exhibits LREE (light rare earth element) enrichment (La_N/Yb_N=9.09) relative to HREE (heavy rare earth element). This metagabbro has a geochemical trend similar to LREE-enriched patterns of ocean island basalt (OIB; Sun & McDonough 1989). Flat-lying REE patterns are similar to those of average N-MORB, displaying that they may have been derived from a fractional asthenospheric mantle and formed in a subduction-related setting (Fig. 8b). Metaophiolite samples have $(Eu/Eu^*)_{CN}$ ratios between 0.70 and 1.84 and slightly exhibit positive Eu anomalies in general. Metadunite samples indicates LREE abundances close to N-MORB.

Discussion

Petrogenesis of the Tozlu metaophiolite

Mineralogical and petrographical results suggest that the Tozlu metaophiolite in the Kazdağ Massif located in northwestern Turkey have a magmatic nature of their protoliths (basalt, Fig. 7a). Subhedral grain shape and lamellar plagioclase grains in less-foliated metagabbros represent the preserved magmatic textures. However, the metamorphic processes

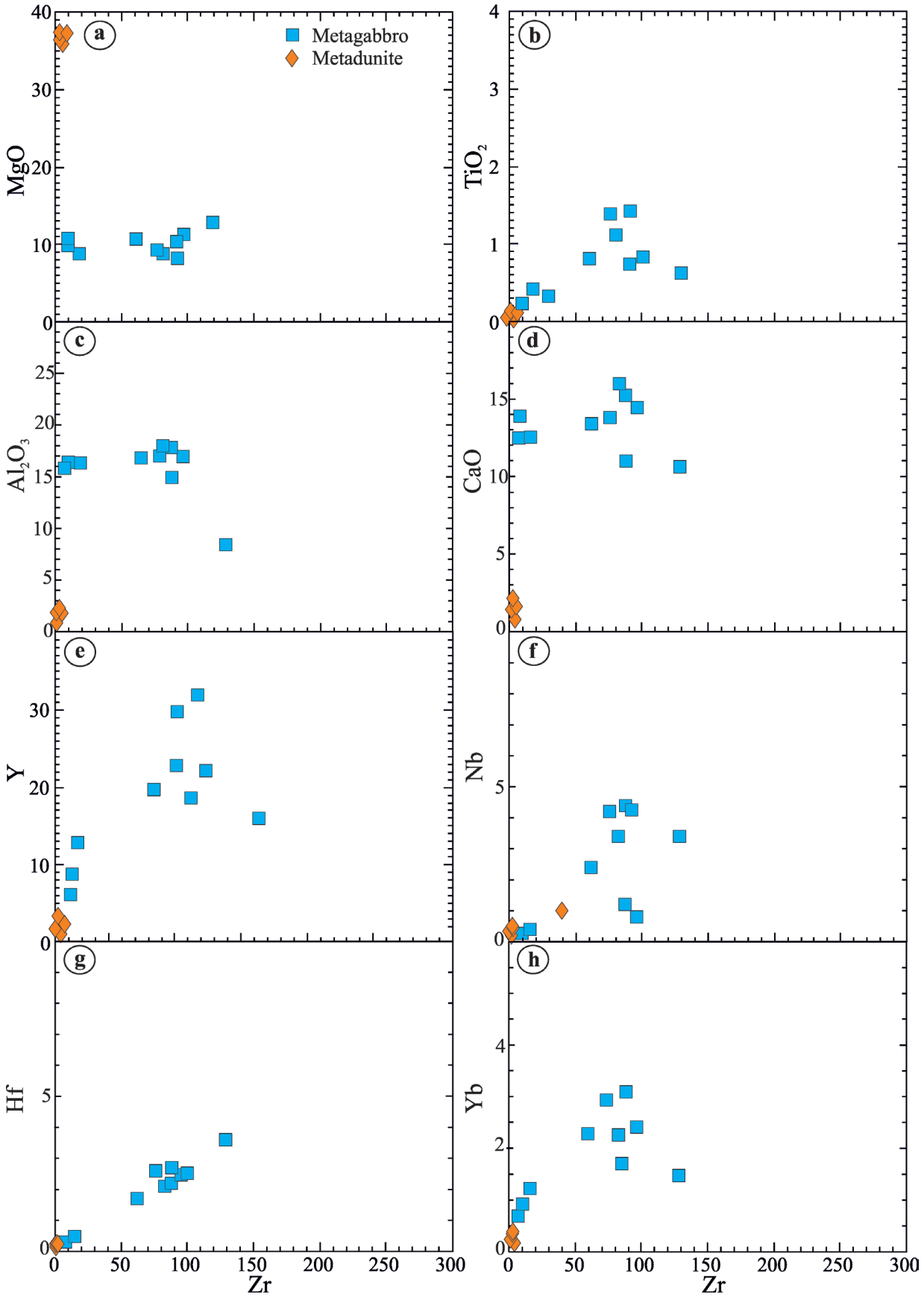

Fig. 6. Variation diagrams of selected major and trace elements versus Zr for the Tozlu metaophiolite (**a**–**h**).

obliterated the magmatic textures of well-foliated amphibolites.

The ratio/ratio plots of incompatible elements in the metagabbro and metadunite samples (Fig. 9) revealed the mantle regions of metaophiolite. Nb/Y ratios of metaophiolite samples are lower than 1 (0.02–0.21) and have an average Nb/Y ratio of 0.11. However, transitional and alkaline basalts have higher Nb/Y ratios (>1) (Pearce & Cann 1973). Ti/Y (29.95–296.92) and Nb/Y (0.01–0.17) ratios exhibit that all of the analyzed samples derived from tholeiitic magma (Fig. 9a). Based on their SiO_2, MgO, CaO, and TiO_2 compositions, these rocks also have a tholeiitic composition, which is very similar to N-MORB. The Sm/Yb versus Ce/Yb plot shows the mantle source of the Tozlu metaophiolite, which separates the Mid-Ocean Ridge Basalt (MORB) and Ocean Island Basalt (OIB) compositions (Fig. 9b). Metagabbros have low Sm/Yb (0.75–1.16) and Ce/Sm (1.60–4.88) ratios, except for one sample (1769), which indicates that they were derived from a more depleted MORB-like mantle source (Fig. 9b). However, sample 1769 has high Sm/Yb (4) and Ce/Sm (7.93) ratio that suggests a derivation from melting of an OIB-like enriched mantle source. The low Sm/Yb (0.42–0.68) and Ce/Sm (2.63–5.56) ratios from the metadunite samples exhibit that these rocks were also derived from a depleted MORB-like mantle source. Moreover, the high Ba/Nb ratios of the metaophiolite samples reflect the subduction-related component (Pearce et al. 1984; Saunders & Tarney 1991). In the diagram of Th/Yb – Ta/Yb including the MORB, OIB array separates intraplate basalts (enriched mantle) and MORB (depleted mantle) sources (Pearce 1982; Fig. 9c). The addition of a subduction component via slab-derived melts causes an increase of Th/Yb in the mantle source (Parlak et al. 2013). The mafic mineral composition of metagabbros suggests that the melting of metagabbros originated in a hydrous mantle source and the water was thus derived from a subducted slab. Aside from one sample (sample 1769), all of the metagabbros have lower Th contents and were derived from a depleted mantle source, which changed by the addition of a subduction component (Fig. 9c). On the other hand, the Th/Yb–Ta/Yb diagram indicates a derivation from an enriched mantle source for most of the metadunite samples (Fig. 9c). This is in concordance with the diagram of Th/Yb versus Nb/Yb, which shows the metaophiolite samples ploting in the volcanic arc array and above the MORB-OIB region. This shows that metaophiolite samples comprise subduction zone components/fluids (Fig. 9d). Th/Yb–Ta/Yb–Nb/Yb ratios designate the influence of a subduction zone regarding the mantle-crust interaction in the melting (Bonev et al. 2023). Therefore, the Th/Yb and Ta/Yb ratios indicate that the metaophiolites had originated due to the metamorphism of MORB-type basaltic protolith during the intra-oceanic subduction or thrusting. These MORB-type tholeiitic products were underplated and accreted to the base of the overriding oceanic plate and then experienced amphibolite-facies metamorphism (Şengün 2022). This amphibolite-facies metamorphism of the Tozlu metaophiolite in the Kazdağ Massif resulted from the northward subduction of the İzmir–Ankara branch of the Neo-Tethyan Ocean under the Sakarya Zone (Şengün & Zack 2016). The Tozlu metaophiolite is considered part of the Paleotethyan Ocean according to the field relations (e.g., Okay et al. 1996; Okay & Satır 2000b; Duru et al. 2004; Erdoğan et al. 2013). However, there is no age data

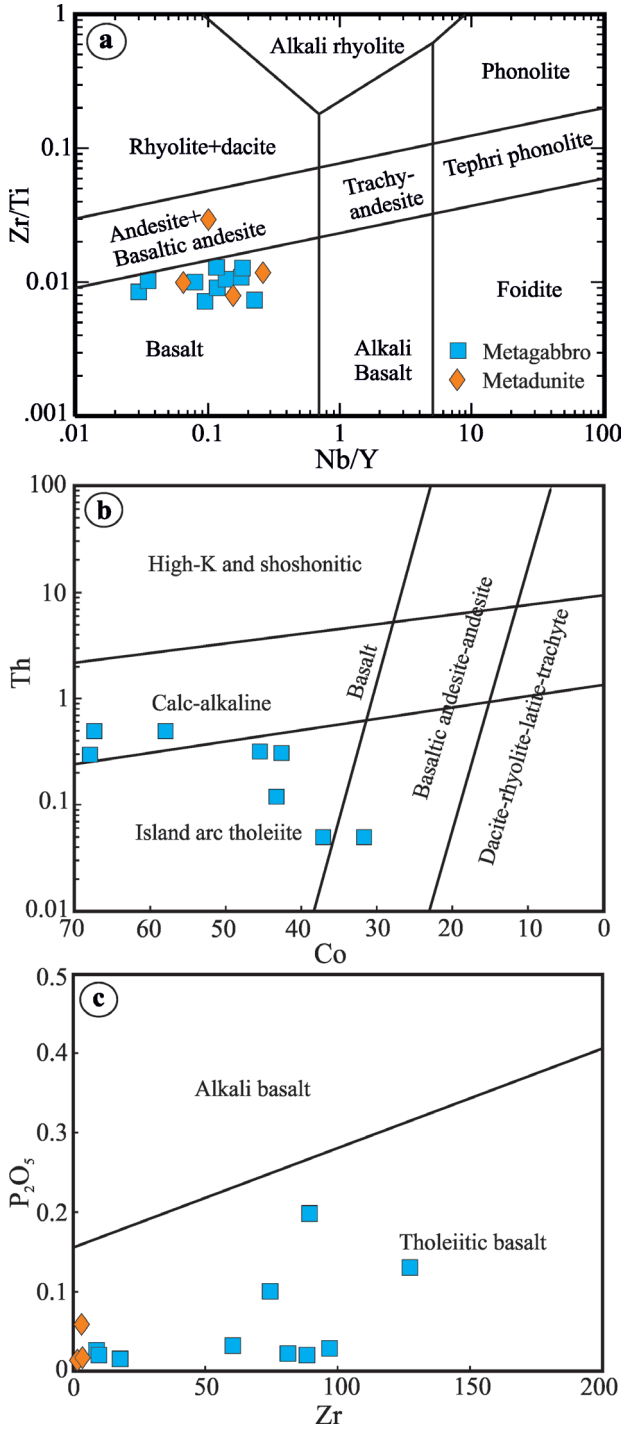

Fig. 7. a — Rock classification diagram of Nb/Y versus Zr/Ti for amphibolites (Pearce 1996); **b** — Th–Co diagram displaying the protolith of amphibolites (Hastie et al. 2007); **c** — P_2O_5 versus Zr discrimination diagram for geochemical affinity (Winchester & Floyd 1976).

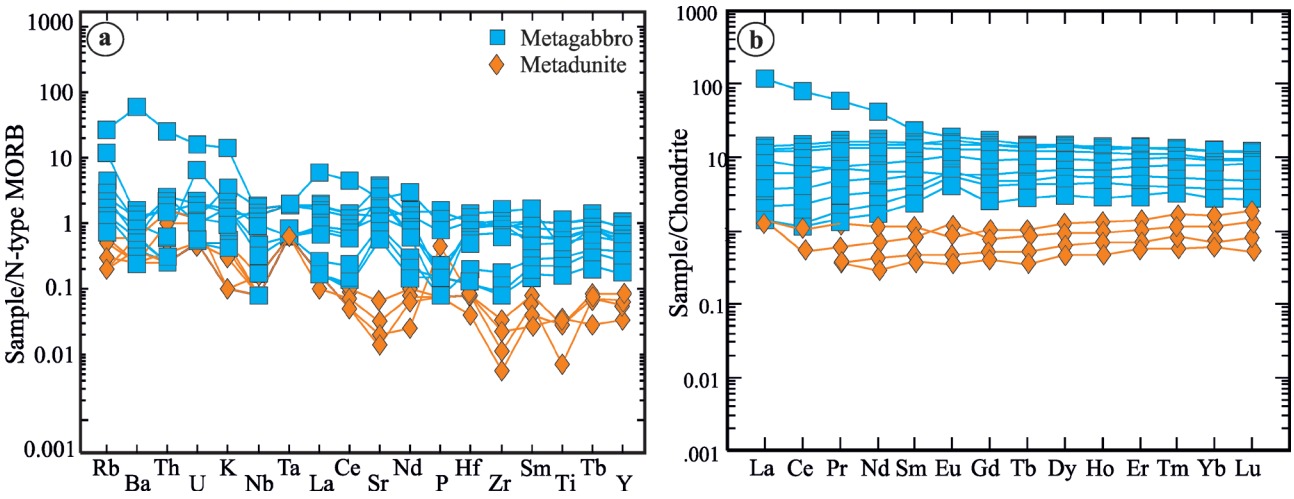

Fig. 8. a — N-MORB normalized multi-element diagram for metaophiolite samples; **b** — Chondrite-normalized rare earth element (REE) diagram. Normalizing values from Sun & McDonough (1989).

Table 2: Rare earth element (ppm) analyses of metaophiolitic rocks from the Tozlu metaophiolite.

	Metadunite				Metagabbro									
Sample no.	**1720**	**1721**	**1730**	**1774**	**1740**	**1741**	**1754**	**1756**	**1760**	**1769**	**1771**	**1775A**	**1775B**	**1777**
ppm														
La	0.5	0.5	0.5	0.3	0.5	4.7	2.2	5.2	0.5	17.5	5.8	2.5	2.7	0.8
Ce	0.5	1	0.5	0.7	1.1	12.8	5.9	14.1	1.2	43.8	13.9	6.8	7.8	2.2
Pr	0.08	0.17	0.05	0.11	0.2	2.02	1.03	2.29	0.25	5.9	1.95	0.95	1.19	0.42
Nd	0.5	0.8	0.2	0.6	1.2	10.5	5.8	11.9	1.6	24.1	9.4	5	6.3	2.4
Sm	0.19	0.26	0.09	0.13	0.54	3.43	2.07	3.59	0.75	5.52	2.85	1.52	2.05	0.91
Eu	0.11	0.07	0.03	0.05	0.38	1.47	0.93	1.32	0.48	1.17	1.16	0.84	1	0.56
Gd	0.23	0.32	0.12	0.31	0.74	4.52	2.79	4.58	1.23	4.36	3.59	2.58	3.11	1.47
Tb	0.05	0.06	0.02	0.05	0.16	0.83	0.55	0.79	0.25	0.6	0.63	0.44	0.6	0.28
Dy	0.36	0.47	0.18	0.42	1.14	5.4	3.66	5.33	1.65	3.31	4.18	2.99	4	2.07
Ho	0.08	0.11	0.04	0.1	0.24	1.18	0.77	1.1	0.38	0.55	0.75	0.65	0.84	0.45
Er	0.25	0.35	0.14	0.26	0.75	3.27	2.32	3.39	1.03	1.43	2.48	1.85	2.31	1.39
Tm	0.04	0.06	0.02	0.05	0.12	0.46	0.35	0.45	0.14	0.22	0.36	0.28	0.34	0.19
Yb	0.28	0.39	0.15	0.31	0.69	2.95	2.28	3	0.92	1.38	2.26	1.74	2.41	1.22
Lu	0.05	0.07	0.02	0.06	0.1	0.45	0.35	0.46	0.14	0.22	0.36	0.3	0.36	0.18
(La/Yb)cn	1.28	0.92	2.39	0.69	0.52	1.14	0.69	1.24	0.39	9.09	1.84	1.03	0.80	0.47
(La/Sm)cn	1.70	1.24	3.59	1.49	0.60	0.89	0.69	0.94	0.43	2.05	1.31	1.06	0.85	0.57
(Gd/Yb)cn	0.68	0.68	0.66	0.83	0.89	1.27	1.01	1.26	1.11	2.61	1.31	1.23	1.07	1.00
(La/Y)cn	1.66	1.14	2.76	0.83	0.55	1.04	0.75	1.09	0.36	7.20	1.73	0.90	0.82	0.41
(Tb/Yb)cn	0.81	0.70	0.61	0.73	1.05	1.28	1.10	1.20	1.24	1.98	1.27	1.15	1.13	1.04
(Tb/Y)cn	1.05	0.87	0.70	0.87	1.12	1.16	1.18	1.05	1.13	1.56	1.19	1.01	1.16	0.91
(Eu/Eu*)cn	1.61	0.74	0.88	0.73	1.84	1.14	1.18	0.99	1.52	0.70	1.11	1.29	1.21	1.47

for the Tozlu metaophiolite so far. Thus, it is not being compared to the other metaophiolitic rocks in Turkey and the surrounding areas. Many ophiolitic rocks in Turkey are Jurassic to Cretaceous in age (e.g., Parlak & Delaloye 1999; Robertson 2002; Çelik et al. 2006, 2019; Parlak et al. 2013; Özkan et al. 2022). On the other hand, Middle–Late Paleozoic magmatic history of metaophiolitic rocks is known in the eastern Rhodope region (e.g., Bonev et al. 2013, 2019, 2023; Bonev 2015; Peytcheva et al. 2018). Therefore, the Tozlu metaophiolite may be correlated with the meta-mafic rocks in the eastern Rhodope region in terms of lithological, mineralogical, and geochemical characteristics.

Tectonic setting

The chemical composition of metaophiolitic rocks, especially incompatible trace and REEs, ensures valuable information on the tectonic setting of their protoliths. Therefore, the trace elements were used for discriminating the tectonic settings of the metaophiolitic rocks. The tectono-magmatic discrimination diagrams define an island arc to spreading ridge settings for the metagabbros and metadunites, where these rocks correspond to MORB and BABB (back-arc basin basalts) with arc-related IAT and CAB (calc-alkaline basalts) areas of (ultra)mafic rocks on the ocean floor (Saunders &

Tarney 1991; Shervais 2001; Bonev et al. 2013; Fig. 10). The V–Ti diagram Shervais (1982) comprises island arc tholeiite (Ti/V≤20), mid-ocean ridge basalts (Ti/V between 20 and 50), and oceanic island basalts (Ti/V>20). The Ti/V ratios of metagabbros range between 5.92 and 71.39, whereas the metadunite samples have Ti/V ratios that vary from 2.61 to 47.94. Metaophiolite samples are plotted on the IAT and MORB-BABB fields based on the diagram of V versus Ti (Wang et al. 2020; Fig. 10a). The protolith of the metaophiolitic rocks can be attributed to the SSZ (supra-subduction zone) origin and were formed in an island arc/back-arc setting. The presence of negative Nb and Ti anomalies in the metaophiolite samples relative to MORB testifies to the characteristics for the subduction-related magmas. The positive Ta, Th anomalies, and high Ba/Nb ratios in metaophiolite imply a connection to arc/back-arc setting. Moreover, the lavas erupted in back-arc fields might plot in MORB/IAT areas displaying evidence for island arc/back-arc origin (e.g., Saunders & Tarney 1991; Pearce 2003; Dilek et al. 2007; Bonev et al. 2023). Metagabbros mostly have IAT affinity, representing the intra-oceanic subduction zone. Similar metamafic rocks were identified from the Armutlu Peninsula in the north of the Sakarya Zone (Özbey et al. 2022; Şengün 2022). Subduction-initiation related ophiolites largely form a separate time trend on this V/Ti diagram, and when the subduction begins, a progression from more MORB-like to more IAT-like magmas develops as the subduction effect increases while the slab subducts far enough to play as a barrier to mantle flow (Pearce 2014).

The immobile trace element tectonic-environment diagrams are shown in Fig. 10b, c, d. The Zr/Y–Zr tectonic discrimination diagram (Pearce & Norry 1979) displays island arc to

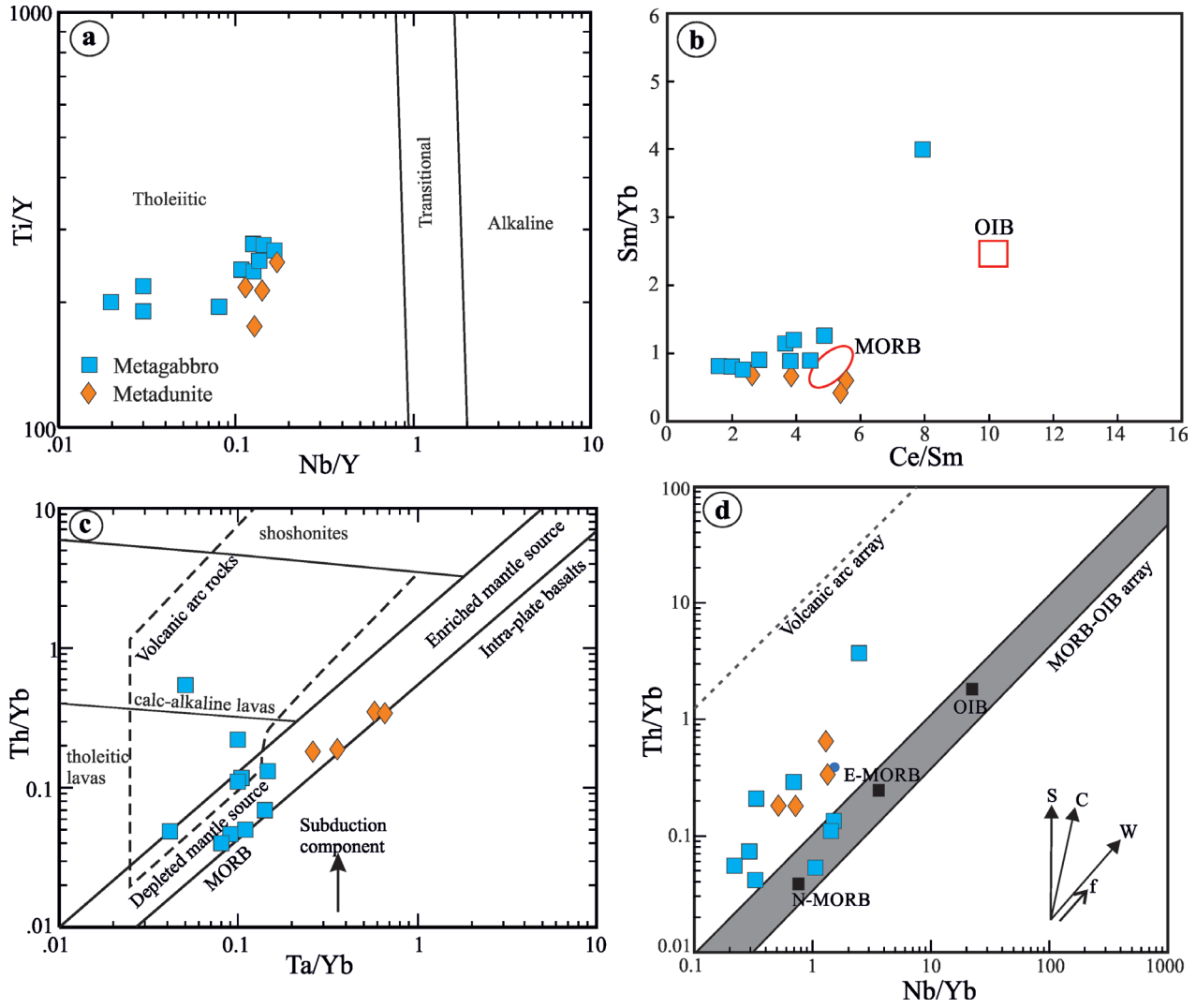

Fig. 9. a — Immobile trace element discrimination diagram of Nb/Y–Ti/Y (from Pearce 1982); **b** — Ce/Sm versus Sm/Yb diagram for source characteristics of metaophiolite samples; **c** — Th/Yb versus Ta/Yb source discrimination diagram (from Pearce 1982); **d** — the diagram of Th/Yb–Nb/Yb for metaophiolite samples (from Pearce 2008). The mantle array includes constructive plate boundary magmas (N-MORB: normal mid-ocean ridge basalts; E-MORB: enriched mid-ocean ridge basalts; and OIB: ocean island basalts). The vectors S, C, W, and f refer the subduction component, crustal contamination, within-plate fractionation, and fractional crystallization, respectively (Pearce 2008).

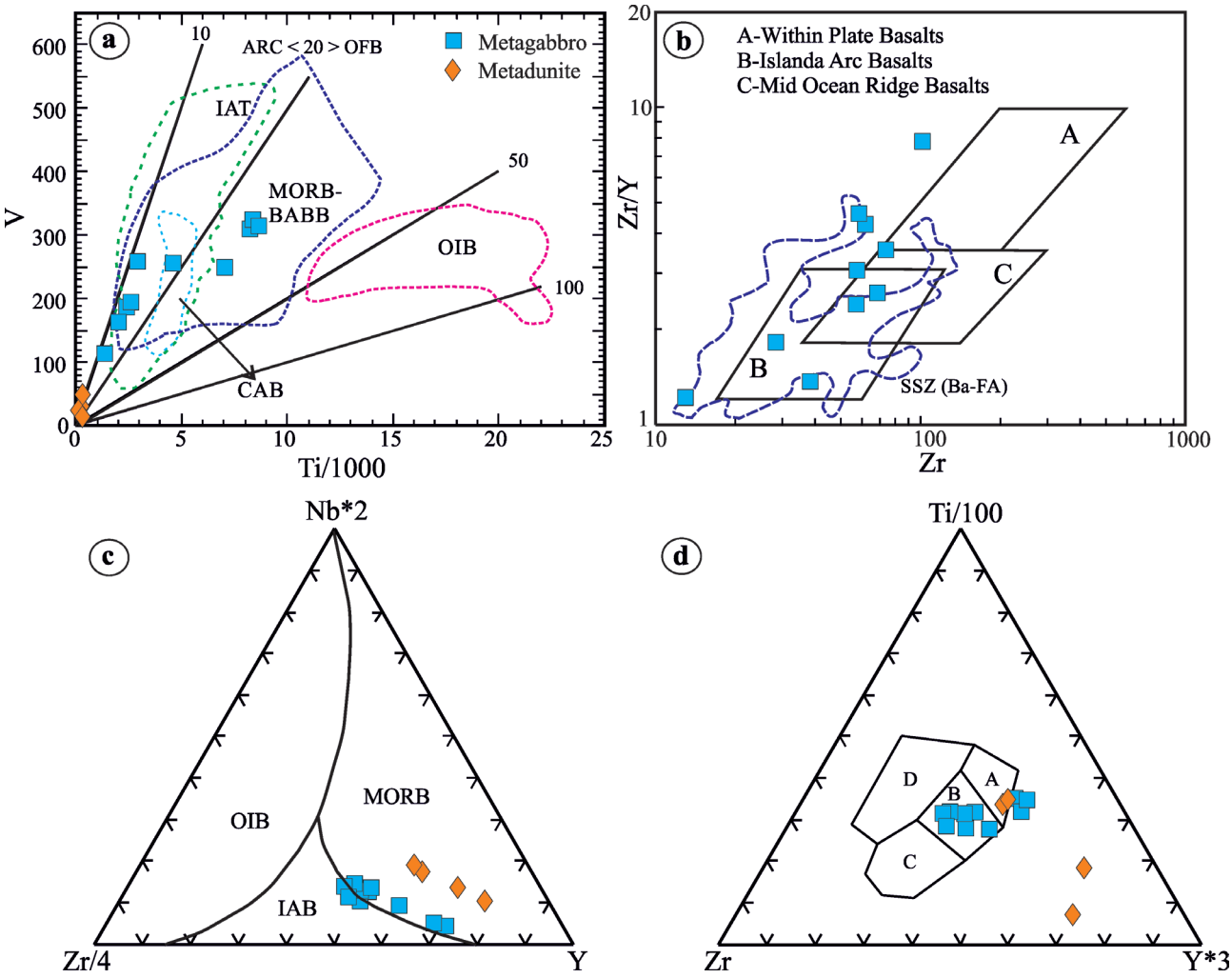

Fig. 10. Tectonic discrimination diagrams of the metaophiolite samples: **a** — V–Ti discrimination diagram displaying fields of IAT (island arc tholeiite), volcanic arc CAB (calc-alkaline basalts), MORB and BABB (mid-ocean ridge basalts and back-arc basin basalts) and OIB (ocean island basalts) from Shervais (1982) modified by Wang et al. (2020); **b** — Zr/Y versus Zr from Pearce & Norry (1979) modified by Furnes et al. (2007); **c** — Nb–Zr–Y discrimination diagram from Vermeesch (2006). OIB: ocean island basalts, IAB: island arc basalts, MORB: mid-ocean ridge basalts; **d** — discrimination diagram of Ti–Zr–Y from Pearce & Cann (1973). A: island arc tholeiite, B: mid-ocean ridge basalts, island arc tholeiite, calc-alkaline basalts, C: calc-alkaline basalts, D: within-plate basalts.

mid-ocean ridge affinities for the metagabbros of the Tozlu metaophiolite (Fig. 10b). Most of the metagabbro samples except for two metagabbros (sample 1769 and sample 1775A) fall in the supra-subduction zone setting. The supra-subduction zone ophiolites were formed by the subduction initiation and then occurred rapid slab rollback, seafloor spreading in the upper plate, and a generation of melt with MORB-like compositions in the fore- to back-arc setting in the early phase of melting (Saunders & Tarney 1991; Dilek & Furnes 2011). The MORB-IAT signatures are well-known in supra-subduction zone ophiolites (e.g., Mposkos et al. 1989; Pearce 2003; Dilek et al. 2007; Dilek & Furnes 2011; Bonev et al. 2013, 2023). The Nb–Zr–Y ternary diagram of Vermeesch (2006) and Ti–Zr–Y ternary diagram of Pearce & Norry (1979) indicate that the metaophiolite samples plot in the field of MORB-island arc basalts (Fig. 10c, d). Trace element geochemistry shows MORB to arc-like supra-subduction zone signatures of the Tozlu metaophiolite. The Tozlu metaophiolite is associated with the metasedimentary succession of platform-type carbonates and migmatized clastic rocks (the Sarıkız unit), which fits the interpretation of SSZ origin. The Tozlu metaophiolite is referred to as a part of the Paleotethyan ocean and associated platform-type succession with metaclastics (Sarıkız unit), which resembles the Mesozoic sequence of the Sakarya continent (Erdoğan et al. 2013). Ultramafic rocks with MORB to supra-subduction zone (SSZ)-like signature occur in the upper unit of the high-grade metamorphic basement in the eastern Rhodope Massif (Bazylev et al.1999; Kolcheva et al. 2000). These metaophiolitic rocks have the MORB/IAT geochemistry of oceanic crust tholeiite protolith (Mposkos et al. 1989). The MORB/IAT affinity of metaophiolitic rocks are interpreted as having protoliths generated in a back-arc rift spreading setting (Bonev et al. 2013, 2023).

Conclusions

The Tozlu metaophiolite and associated metacarbonate and migmatized metaclastics occur as a tectonic slice in the Kazdağ Massif located in the northwestern part of Turkey. The combination of the geochemistry (major, trace, and rare earth elements) with the petrography of the Tozlu metaophiolite in the Kazdağ Massif provided significant knowledge about protolith, petrogenesis, source characteristics, and the tectonic setting of northwest Turkey. The Tozlu metaophiolite is mainly composed of metagabbro, banded amphibolite, metadunite and serpentinite, which experienced amphibolite-facies metamorphism. Trace element geochemistry displays tholeiitic affinity of the igneous protoliths of basaltic composition. Geochemistry of the metaophiolitic rocks indicates that the metaophiolitic rocks were derived from a tholeiitic magma and generated in an island arc tectonic setting. Various tectono-magmatic discrimination diagrams of trace elements define a mid-ocean ridge basalt (MORB) to volcanic arc (IAT) affinity for the Tozlu metaophiolite, which is certified by LILE enrichment, HFSE, and HREE depletion relative to N-MORB, as well as Nb and Ti negative anomalies. The tholeiitic metaophiolitic rocks resulted from the metamorphism of an island arc-type basaltic protolith and indicate a subduction zone component based on the Th/Yb and Ta/Yb ratios. The Tozlu metaophiolite with MORB/IAT affinity testifies to the supra-subduction zone origin in an island arc/back-arc settings. The Sarıkız unit is represented by the thick, platform-type, highly-recrystallized, white marbles that alternate migmatized metasedimentary rocks unconformably and overlie the Tozlu metaophiolite, which represent the deposits from different arc/back-arc regions (e.g., fore-arc or intra-arc). This is consistent with the interpretation of the SSZ tectonic setting.

Acknowledgements: The Scientific Research Coordination Unit of Çanakkale Onsekiz Mart University supported this study under project number FHD-2022–4001. Constructive reviews by Nikolay Bonev and Milan Kohút helped to clarify the picture and considerably improved the manuscript.

References

Aygül M., Topuz G., Okay A.I., Satır M. &Meyer H.P. 2012: The Kemer Metamorphic Complex (NW Turkey), a subducted continental margin of the Sakarya Zone. *Turkish Journal of Earth Sciences* 21, 19–35. https://doi.org/10.3906/yer-1006-14

Aysal N., Öngen A.S., Peytcheva I. & Keskin M. 2012: Origin and evolution of the Havran Unit, Western Sakarya basement (NW Turkey): new LA-ICP-MS U–Pb dating of the metasedimentary–metagranitic rocks and possible affiliation to Avalonian microcontinent. *Geodinamica Acta* 25, 226–247. https://doi.org/10.1080/09853111.2014.882536

Bazylev B.A., Zakariadze G.S., Zeljazkova-Panayotova M.D., Kolcheva K., Oberhansli R. & Solovieva N.V. 1999: Petrology of ultrabasites from the ophiolitic association in crystalline basement of the Rhodope Massif. *Petrology* 7, 191–212 (in Russian).

Beccaletto L. & Jenny C. 2004: Geology and Correlation of the Ezine Zone: A Rhodope Fragment in NW Turkey? *Turkish Journal of Earth Sciences* 13, 145–176.

Beccaletto L., Bartolini A.C., Martini R., Hochuli P.A. & Kozur H. 2005: Biostratigraphic data from Çetmi Melange, northwest Turkey: Palaeogeographic and tectonic implications. *Palaeogeography, Palaeoclimatology, Palaeoecology* 221, 215–244. https://doi.org/10.1016/j.palaeo.2005.02.011

Beccaletto L., Bonev N., Bosch D. & Bruguier O. 2007: Record of a Paleogene syn-collisional extension in the north Aegean Sea: evidence from the Kemer micaschists (NW Turkey). *Geological Magazine* 144, 393–400. https://doi.org/10.1017/S001675680700310X

Bingöl E. 1969: Central of the Kazdağ Massif and geology of the southeastern part. *Bulletin of the Mineral Research and Exploration* 72, 110–123 (in Turkish).

Bonev N. 2015: Protoliths and metamorphic events in the high-grade metamorphic basement of the Eastern Rhodope: constraints from U–Pb zircon geochronology. In: Proceedings of Annual Conference of the Bulgarian Geological Society "Geosciences 2015", 57–58.

Bonev N., Ovtcharova-Schaltegger M., Moritz R., Marchev P. & Ulianov A. 2013: Peri Gondwanan Ordovician crustal fragments in the high-grade basement of the Eastern Rhodope Massif, Bulgaria: evidence from U-Pb LA-ICP-MS zircon geochronology and geochemistry. *Geodinamica Acta* 26), 207–229. https://doi.org/10.1080/09853111.2013.858942

Bonev N., Filipov P. & Raicheva R. 2019: Age of the metaophiolites in the Eastern Rhodope Massif: Prototethys vs. Paleotethys connection. In: Goldschmid Abstracts, abstract 325.

Bonev N., Dotseva Z. & Filipov P. 2023: Geochemistry and tectonic significance of metamorphosed mafic ophiolitic rocks in the upper high-grade basement unit of the eastern Rhodope Massif (Bulgaria–Greece). *Geologica Carpathica* 74, 23–39. https://doi.org/10.31577/GeolCarp.2023.05

Cavazza W., Okay A.I. & Zattin M. 2009: Rapid early-middle Exhumation of the Kazdağ Massif (western Anatolia). *International Journal of Earth Sciences* 98, 1935–1947. https://doi.org/10.1007/s00531-008-0353-9

Çelik Ö.F., Delaloye M. & Feraud G. 2006: Precise ^{40}Ar–^{39}Ar ages from the metamorphic sole rocks of the Tauride Belt Ophiolites, southern Turkey: implications for the rapid cooling history. *Geological Magazine* 143, 213–227. https://doi.org/10.1017/S0016756805001524

Çelik Ö.F, Topuz G., Billor Z. & Özkan M. 2019: Middle Jurassic subduction-related ophiolite fragment in Triassic accretionary complex (Mamu Dağı ophiolite, Northern Turkey*). International Geology Review* 61, 2021–2035. https://doi.org/10.1080/00206814.2019.1578109

Dilek Y. & Furnes H. 2011: Ophiolite genesis and global tectonics: Geochemical and tectonic fingerprinting of ancient oceanic lithosphere. *Geological Society of America Bulletin* 123, 387–411. https://doi.org/10.1130/B30446.1

Dilek Y., Furnes H. & Shallo M. 2007: Suprasubduction zone ophiolite formation along the periphery of Mesozoic Gondwana. *Gondwana Research* 11, 453–475. https://doi.org/10.1016/j.gr.2007.01.005

Duru M., Pehlivan Ş., Şentürk Y., Yavaş F. & Kar H. 2004: New Results on the Lithostratigraphy of the Kazdağ Massif in Northwest Turkey. *Turkish Journal of Earth Science* 13, 177–186.

Duru M., Pehlivan Ş., Okay A.İ., Şentürk Y. & Kar H. 2012: Pre-Tertiary geology of Biga Peninsula. In: Yüzer E. & Tunay G. (eds): General and Economic Geology of Biga Peninsula. *Bulletin of the Mineral Research and Exploration Special Series* 28, *MTA*, Ankara, 7–74 (in Turkish).

Erdoğan B., Akay E., Hasözbek A., Satır M. & Siebel W. 2013: Stratigraphy and tectonic evolution of the Kazdağ Masif (NW Ana-

tolia) based on field studies and radiometric ages. *International Geology Review* 55, 2060–2082. https://doi.org/10.1080/00206814.2013.818756

Frey F.A., Green D.H. & Roy S.D. 1978: Integrated models of basalt petrogenesis: a study of quartz tholeiites to olivine melilitites from South Eastern Australia utilizing geochemical and experimental petrological data. *Journal of Petrology* 19, 463–513.

Furnes H., Wit M.J., Staudigel H., Rosing M. & Muehlenbachs K. 2007: A vestige of earth's oldest ophiolite. *Science* 315, 1704–1707. https://doi.org/10.1126/science.1139170

Galoyan G., Rolland Y., Sosson M., Corsini M., Billo S., Verati C. & Melkonyan R. 2009: Geology, geochemistry and $^{40}Ar/^{39}Ar$ dating of Sevan ophiolites (Lesser Caucasus, Armenia): evidence for Jurassic Back-arc opening and hot spot event between the South Armenian Block and Eurasia. *Journal of Asian Earth Sciences* 34, 135–153. https://doi.org/10.1016/j.jseaes.2008.04.002

Gartzos E., Dietrich V.J., Migiros G., Serelis K. & Lymperopoulou T. 2009: The origin of amphibolites from metamorphic soles beneath the ultramafic ophiolites in Evia and Lesvos (Greece) and their geotectonic implication. *Lithos* 108, 224–242. https://doi.org/10.1016/j.lithos.2008.09.013

Hassig M., Rolland Y., Sosson M., Galoyan G., Sahakyan L., Topuz G., Çelik Ö.F., Avagyan A. & Müller C. 2013. Linking the NE Anatolian and Lesser Caucasus ophiolites: evidence for large-scale obduction of oceanic crust and implications for the formation of the Lesser Caucasus–Pontides Arc. *Geodinamica Acta* 26, 311–330. https://doi.org/10.1080/09853111.2013.877236

Hastie A., Kerr A., Pearce J. & Mitchell S. 2007: Classification of Altered volcanic island arc rocks using immobile trace elements: Development of the Th co discrimination diagram. *Journal of Petrology* 48, 2341–2357. https://doi.org/10.1093/petrology/egm062

Höhn M., Bröcker M. & Berndt J. 2022: The Jurassic meta-ophiolitic rocks of Cape Steno, Andros, Greece: a high-pressure/low-temperature mélange with Pelagonian affinity in the Cycladic Blueschist unit? *International Journal of Earth Sciences* 111, 949–968. https://doi.org/10.1007/s00531-022-02161-w

Kolcheva K., Haydoutov I. & Daieva L. 2000: Dismembered ultramafic ophiolites from the Avren synform, Eastern Rhodopes. *Geochemistry, Mineralogy and Petrology* (Sofia) 37, 27–38.

Liati A., Gebauer D. & Fanning C.M. 2004. The age of ophiolitic rocks of the Hellenides (Vourinos, Pindos, Crete): first U–Pb ion microprobe (SHRIMP) zircon ages. *Chemical Geology* 207, 171–188. https://doi.org/10.1016/j.chemgeo.2004.02.010

Meinhold G., Kostopoulos D., Frei D., Himmerkus F. & Reischmann T. 2010: U–Pb LA-SF ICP-MS zircon geochronology of the Serbo–Macedonian Massif, Greece: Paleotectonic constraints for Gondwana-derived terranes in the Eastern Mediterranean. *International Journal of Earth Sciences* 99, 813–832. https://doi.org/10.1007/s00531-009-0425-5

Mposkos E., Perdikatsis B. & Liati A. 1989: Geochemical investigation of amphibolites from eastern and central Rhodope. *Bulletin of the Geological Society of Greece* 23, 413–425.

M.T.A. 2012: General and economic geology of the Biga Peninsula. *Special Publication Series* 28, 1–326 (in Turkish).

Okay A.İ. & Göncüoğlu M.C. 2004: The Karakaya Complex: A Review of Data and Concepts. *Turkish Journal of Earth Sciences* 13, 77–95.

Okay A.İ. & Satır M. 2000a: Upper Cretaceous Eclogite – Facies Metamorphic Rocks from the Biga Peninsula, Northwest Turkey. *Turkish Journal of Earth Sciences* 9, 47–56.

Okay A. İ. & Satır M. 2000b: Coeval plutonism and metamorphism in a latest Oligocene metamorphic core complex in Northwest Turkey. *Geological Magazine* 137, 495–516. https://doi.org/10.1017/S0016756800004532

Okay A.İ. & Tüysüz O. 1999: Tethyan sutures of northern Turkey. *Geological Society of London Special Publications* 156, 475–515. https://doi.org/10.1144/GSL.SP.1999.156.01.22

Okay A.İ., Siyako M. & Bürkan K.A. 1991: Geology and tectonic evolution of the Biga Peninsula. In: Dewey J.F. (Ed.): Special Issue on Tectonics. *Bulletin of the Technical University of Istanbul* 44, 191–255.

Okay A.İ, Satır M., Maluski H., Siyako M., Monie P., Metzger R. & Akyüz S. 1996: Paleo and Neotethyan events in northwest Turkey. In: Yin A. & Harrison M. (eds): Tectonics of Asia. *Cambridge University Press*, Cambridge, 420–441.

Okay A.İ., Tansel İ. & Tüysüz O. 2001: Obduction, subduction and collision as reflected in the Upper Cretaceous–Lower Eocene sedimentary record of western Turkey. *Geological Magazine* 138, 117–142. https://doi.org/10.1017/S0016756801005088

Okay A.İ., Satır M. & Siebel W. 2006: Pre-Alpine orogenic events in the Eastern Mediterranean region. In: Gee D.G. & Stephenson R.A. (eds): European Lithosphere Dynamics. *Geological Society of London, Memoirs* 32, 389–405. https://doi.org/10.1144/GSL.MEM.2006.032.01.23

Okay A.İ., Altiner D., Sunal G., Aygül M., Akdoğan R., Altiner S. & Simmons M. 2018: Geological evolution of the Central Pontides. *Geological Society of London Special Publications* 464, 33–67. https://doi.org/10.1144/SP464.3

Özbey Z., Karslıoğlu Ö. & Aysal N. 2022: First evidence for the subduction initiation and boninitic magmatism from the Armutlu Peninsula (NW Turkey): geodynamic significance for the Cadomian magmatic arc system of the Gondwanan margin. *International Geology Review* 64, 2497–2521. https://doi.org/10.1080/00206814.2021.1986680

Özkan M., Çelik Ö.M., Çörtük, R.M., Topuz G., Zack T. & Çubukçu E. 2022: Early Middle Jurassic metamorphic and non-metamorphic supra-subduction zone ophiolite fragments in a Late Cretaceous ophiolitic mélange (northern Turkey): implications for long-lived and supra-subduction zone ophiolite formation. *International Journal of Earth Sciences* 111, 2391–2408. https://doi.org/10.1007/s00531-022-02235-9

Parlak O. & Delaloye M. 1999: Precise $^{40}Ar/^{39}Ar$ ages from the metamorphic sole of the Mersin ophiolite (Southern Turkey): *Tectonophysics* 301, 145–158.

Parlak O., Çolakoğlu A., Dönmez C., Sayak H., Yıldırım N., Türkel A. & Odabası İ. 2013: Geochemistry and tectonic significance of ophiolites along the İzmir–Ankara–Erzincan Suture Zone in northeastern Anatolia. In: Robertson A.H.F., Parlak O. & Ünlügenç U.C. (eds): Geological Development of Anatolia and the Easternmost Mediterranean Region, *Geological Society London Special Publications* 372, 75–105. https://doi.org/10.1144/SP372.7

Pearce J.A. 1982: Trace element characteristics of lavas from destructive plate boundaries. In: Thorpe R.S. (Ed.): Andesites: Orogenic Andesites and Related Rocks. *John Wiley and Sons*, Chichester, 525–548.

Pearce J.A. 1996: A users guide to basalt discrimination diagrams. In: Wyman D.A. (Ed.): Trace element geochemistry of volcanic rocks: Applications for massive sulfide exploration. *Geological Association of Canada*, *Short Course Notes* 12,79–113.

Pearce J.A. 2003. Supra-subduction zone ophiolites: The search for modern analogues. In: Dilek Y. & Newcomb S. (eds.): Ophiolite concept and the evolution of geological thought. *Geological Society of America Special Paper* 373, 269–293. https://doi.org/10.1130/0-8137-2373-6.269

Pearce J.A. 2008: Geochemical fingerprinting of oceanic basalts with applications to ophiolite classification and the search for Archean oceanic crust. *Lithos* 100, 14–48. https://doi.org/10.1016/j.lithos.2007.06.016

Pearce J.A. 2014: Immobile element fingerprinting of ophiolites. *Elements* 10, 101–108. https://doi.org/10.2113/gselements.10.2.101

Pearce J.A. & Cann J.R. 1973: Tectonic setting of basic volcanic rocks determined using trace element analysis. *Earth and Planetary Science Letters* 19, 290–300.

Pearce J.A. & Norry M.J. 1979: Petrogenetic implications of Ti, Zr, Y and Nb variations in volcanic rocks. *Contribution to Mineralogy and Petrology* 69, 33–47.

Pearce J.A. & Peate D.W 1995: Tectonic implications of the composition of volcanic arc magmas. *Annual Review of Earth Sciences* 23, 251–285.

Pearce J.A., Lippard S.J. & Roberts S. 1984: Characteristics and tectonic significance of supra-subduction zone ophiolites. In: Kokelaar B.P. & Howells M.F. (eds): Marginal Basin Geology: Volcanic and Associated Sedimentary and Tectonic Processes in Modern and Ancient Marginal Basins. *Geological Society of London Special Publication* 16, 77–94.

Peytcheva I., von Quadt A., Macheva L., Kolcheva K. & Sarov S. 2018: Relics of Devonian oceanic lithosphere in Byala Reka dome, Eastern Rhodopes: Evidence from zircon U–Pb dating and Hf-isotope tracing. *Comptes Rendus de l'Academie bulgare des Sciences* 71, 1657–1664. https://doi.org/10.7546/CRABS.2018.12.10

Polat A., Hofmann A.W. & Rosing M.T. 2002: Boninite like volcanic rocks in the 3.7–3.8 Ga Isua greenstone belt, West Greenland: Geochemical evidence for intra-oceanic subduction zone processes in the early Earth. *Chemical Geology* 184, 231–254. https://doi.org/10.1016/S0009-2541(01)00363-1

Robertson A.H.F. 2002: Overview of the genesis and emplacement of Mesozoic ophiolites in the Eastern Mediterranean Tethyan region. *Lithos* 65, 1–67. https://doi.org/10.1016/S0024-4937(02)00160-3

Robertson A.H.F. 2004: Development of concepts concerning the genesis and emplacement of Tethyan ophiolites in the Eastern Mediterranean and Oman regions: *Earth Science Review* 66, 331–387. https://doi.org/10.1016/j.earscirev.2004.01.005

Robertson A.H.F. 2012: Late Palaeozoic–Cenozoic tectonic development of Greece and Albania in the context of alternative reconstructions of Tethys in the Eastern Mediterranean region: *International Geology Review* 54, 373–454. https://doi.org/10.1080/00206814.2010.543791

Robertson A.H.F., Parlak O. & Ustaömer T. 2009: Mélange genesis and ophiolite emplacement related to subduction of the northern margin of the Tauride-Anatolide continent, central and western Turkey. In: Van Hinsbergen D.J., Edwards M.A. & Govers R. (eds): Collision and collapse at the Africa-Arabia-Eurasia subduction zone. *Geological Society London Special Publications*, London 311, 9–66. https://doi.org/10.1144/SP311.2

Robertson A.H.F., Parlak O., Ustaömer T., Taslı K., İnan N., Dumitrica P. & Karaoğlan F. 2014: Subduction, ophiolite genesis and collision history of Tethys adjacent to the Eurasian continental margin: new evidence from the Eastern Pontides, Turkey. *Geodinamica Acta* 26, 230–293. https://doi.org/10.1080/09853111.2013.877240

Rolland Y., Galoyan G.H., Bosch D., Sosson M., Corsini M., Fornari M. & Vérati C. 2009: Jurassic Back-arc and hot-spot related series in the Armenian ophiolites – implications for the obduction process. *Lithos* 112, 163–187. https://doi.org/10.1016/j.lithos.2009.02.006

Saunders A. & Tarney J. 1991: Back-arc basins. In: Floyd P.A. (Ed.): Oceanic basalts. *Blackie*, Glasgow, 219–263.

Şengör A.M.C & Yılmaz Y. 1981: Tethyan Evolution of Turkey: A Plate Tectonic Approach. *Tectonophysics* 75, 181–241.

Şengün F. 2022: Geochemistry and Tectonic Setting of Amphibolites in the Pamukova Metamorphics from the Armutlu Peninsula, NW Turkey. *Arabian Journal of Earth Sciences* 15, 605. https://doi.org/10.1007/s12517-022-09939-x

Şengün F. & Koralay O.E. 2017: Early Variscan magmatism along the southern margin of Laurasia: Geochemical and geochronological evidence from the Biga Peninsula, NW Turkey. *International Journal of Earth Sciences* 106, 811–826. https://doi.org/10.1007/s00531-016-1334-z

Şengün F. & Zack T. 2016: Trace element composition of rutile and Zr-in-rutile thermometry in meta-ophiolitic rocks from the Kazdağ Massif, NW Turkey. *Mineralogy and Petrology* 110, 547–560. https://doi.org/10.1007/s00710-016-0433-7

Şengün F., Yigitbas E. & Tunç İ.O. 2011: Geology and Tectonic Emplacement of Eclogite and Blueschist, Biga Peninsula, Northwest Turkey. *Turkish Journal of Earth Sciences* 20, 273–285. https://doi.org/10.3906/yer-0912-75

Şengün F., Koralay O.E. & Kristoffersen M. 2020: Zircon U–Pb age and Hf isotopic composition of the Carboniferous Gönen granitoid in the western Sakarya Zone of Turkey. *Turkish Journal of Earth Sciences* 29, 617–628. https://doi.org/10.3906/yer-1910-7

Shervais J.W. 1982: Ti–V plots and the petrogenesis of modern ophiolitic lavas. *Earth and Planetary Science Letters* 57, 101–118.

Shervais J.W. 2001: Birth, dead, and resurrection: The life cycle of supra-subduction zone ophiolites. *Geochemistry Geophysics Geosystem* 2, 2000GC000080. https://doi.org/10.1029/2000GC000080

Sosson M., Rolland Y., Danelian T., Muller C., Melkonyan R., Adamia S., Babazadeh V., Kangarli T., Avagyan A., Galoyan G. & Mosar J. 2010: Subductions, obduction and collision in the Lesser Caucasus (Armenia, Azerbaijan, Georgia), new insights. *Geological Society of London Special Publications* 340, 329–352. https://doi.org/10.1144/SP340.14

Sun S.S. & McDonough W.F. 1989: Chemical and isotopic systematics of ocean basalts: implications for mantle composition and processes. In: Saunders A.D. & Norry M.J. (eds): Magmatism in Ocean Basins. *Geological Society London Special Publication* 42, 313–345.

Sun S.S. & Nesbitt R.W. 1978: Petrogenesis of Archean ultrabasic and basic volcanics: evidence from the rare earth elements. *Contribution to Mineralogy and Petrology* 65, 301–325.

Sunal G. 2012: Devonian magmatism in the western Sakarya Zone, Karacabey Region, NW Turkey. *Geodinamica Acta* 25, 183–201. https://doi.org/10.1080/09853111.2013.858947

Topuz G., Çelik Ö.F., Şengör A.M.C., Altıntaş İ.E., Zack T., Rolland Y. & Barth M. 2013: Jurassic ophiolite formation and emplacement as backstop to a subduction accretion complex in the Northeast Turkey, the Refahiye ophiolite, and relation to Balkan ophiolites. *American Journal of Sciences* 313, 1054–1087. https://doi.org/10.2475/10.2013.04

Ustaömer T. & Robertson A.H.F. 2010. Late Palaeozoic-Early Cenozoic tectonic development of the Eastern Pontides (Artvin area), Turkey: stages of closure of Tethys along the southern margin of Eurasia. *Geological Society of London Special Publications* 350, 49–74. https://doi.org/10.1144/SP340.13

Vermeesch P. 2006: Tectonic discrimination diagrams revisited. *Geochemistry, Geophysics, Geosystems,* 7, 1–55. https://doi.org/10.1029/2005GC001092

Wang X., Lang X., Tang J., Deng Y., Hel Q., Xiel F., Lil L., Yin Q., Lil Z., Li Z., Yang Z., Dong S., Ding F., Wang Z. & Huang Y. 2020: Early carboniferous back-arc rifting-related magmatism in Southern Tibet: Implications for the history of the Lhasa Terrane separation from Gondwana. *Tectonics* 39, e2020TC006237. https://doi.org/10.1029/2020TC006237

Whitney D.L. & Evans B.W. 2010: Abbreviations for names of rock-forming minerals. *American Mineralogist* 95, 185–187. https://doi.org/10.2138/am.2010.3371

Wilson M. 1989: Igneous petrogenesis. *Chapman and Hall*, London, 1–466.

Winchester J.A. & Floyd P.A. 1976: Geochemical magma type discrimination, application to altered and metamorphosed basic igneous rocks. *Earth and Planetary Science Letters* 28, 459–469.